Temperature-dependent Fermi surface of the misfit cobaltite $[Bi_2Sr_2O_4]_{0.51}CoO_2$: A comparison with $[Bi_2Ba_2O_4]_{0.50}CoO_2$

Sho-ichi Takakura,[1] Isamu Yamamoto,[2] Emi Koga,[1] Fusao Ichikawa,[3] Junpei Azuma,[2] and Makoto Maki[1]
[1]*Department of Physics, Saga University, Saga 840-8502, Japan*
[2]*Synchrotron Light Application Center, Saga University, Saga 840-8502, Japan*
[3]*Department of Physics, Kumamoto University, Kumamoto 860-8555, Japan*
(Received 8 January 2016; revised manuscript received 4 March 2016; published 14 April 2016)

Angle-resolved photoemission spectroscopy has been performed to investigate the Fermi surface (FS) and the electronic structure of misfit cobaltites, by comparing $[Bi_2Sr_2O_4]_pCoO_2$ with $[Bi_2Ba_2O_4]_{0.50}CoO_2$. In $[Bi_2Sr_2O_4]_{0.51}CoO_2$, we observed a suppression of spectral weight near the Fermi energy. Nevertheless, the FS can be mapped out by measuring the photoelectron intensity distribution. The FS size changes with temperature. Additionally, results show that the electronic band structure at a higher binding energy was changed by changing the sample temperature. Our results provide insight into the characteristics of the pseudogap state in the misfit-layered cobaltites. The unusual properties are probably related to the local deformations of the incommensurate structure.

DOI: 10.1103/PhysRevB.93.165118

I. INTRODUCTION

Layered materials provide opportunities to develop future electronic devices because of their hybrid structure combined with atomic layers of different types. Layered cobaltites, which exhibit large values of the Seebeck coefficient, have attracted great interest for their potential use in thermoelectricity generation devices [1–3]. Actually, Na_xCoO_2, $Ca_3Co_4O_9$, and $[Bi_2M_2O_4]_pCoO_2$ (M = Ca, Sr, Ba) all contain a triangular CoO_2 block structure. The 3*d* electrons of cobalt ions having multiple oxidation states that play a fundamentally important role in driving the unique property on the border between the localized and itinerant states. Actually, pseudogap phenomena and charge ordering have been observed experimentally in conjunction with a change in the valence state of cobalt [4–6]. However, the origin of the localization remains unclear. Coulomb repulsion between the 3*d* electrons is one interesting candidate [7–9]. Conversely, when the cobalt is close to a trivalent (nonmagnetic) state, it seems that the unusual magnetic properties become prominent [10,11]. Temperature-dependent transport behavior is also a topic of discussion [12,13]. Interactions with the neighboring layers (or atoms) constitute another issue. In Na_xCoO_2, possible charge ordered states have been discussed in relation to the electrostatic potential of the neighboring sodium ions [14].

Angle-resolved photoemission spectroscopy (ARPES) is a powerful technique to visualize the electronic structure in momentum space. We took ARPES measurements of $[Bi_2Sr_2O_4]_pCoO_2$, which comprises two alternating sublattices, the CoO_2 and rocksalt (RS) structures. Because of van der Waals bonding between the BiO layers, the cleaved surface is ensured to be clean and stable, which constitutes a great advantage for ARPES measurements. The in-plane resistivity of $[Bi_2Sr_2O_4]_pCoO_2$ has been known to exceed the Mott-Ioffe-Regel limit at moderate temperatures. It exhibits an anomalous upturn below about 100 K. Although the temperature dependence of the Hall coefficient is consistent with this phenomenon [15], the mechanism has not been established. In this material, the lattice lengths of the CoO_2 and RS layers are incommensurate along the *b* direction. From the ARPES or the scanning tunneling microscopy (STM) measurements, non-negligible effects of the lattice mismatch on the electronic state have been pointed out [16,17].

As described in this paper, we present detailed ARPES measurements of the misfit cobaltite $[Bi_2Sr_2O_4]_{0.51}CoO_2$ (BSCO), comparing with results for $[Bi_2Ba_2O_4]_{0.50}CoO_2$ (BBCO), which has a commensurate match between the two sublattices. As is well known, the Ba system exhibits different properties from the Sr one, which includes a metallic behavior, a positive magnetoresistance, a weak Curie-Weiss behavior, and so on. First, we show that the spectral weight near the Fermi level E_F is suppressed in BSCO in contrast to that in BBCO. Nonetheless, the Fermi surface (FS) can be displayed by accurately mapping the nonuniformity in the photoelectron intensity distribution. The result implies that the FS does not disappear in the so-called pseudogap state of BSCO. As the temperature decreases, although the density of state at E_F becomes lower, the FS size seems to increase. These paradoxical results might be explained by the following observations: The valence band structure is modified by the change in temperature, and it is related to the change in the local environment around the oxygen atoms. These are regarded as being attributable to the lattice deformation brought about by the mismatch of thermal expansion coefficients between the two sublattices. Our experimentally obtained results suggest that the incommensurate structure of BSCO is not rigid but flexible, which gives rise to the anomalous electronic properties of this compound.

II. EXPERIMENTS

Single crystals were synthesized using a self-flux method with an Al_2O_3 crucible [18]. To standardize the oxygen contents, crystals were annealed in an argon atmosphere at 600°C for 48 h. The inset of Fig. 1(a) shows x-ray $(0,0,l)$ diffraction patterns. No detectable contamination of any impurity phase was observed. Figure 1(a) shows the in-plane resistivity, comparing with that of BBCO. Experiments were conducted at the beamline BL13 at the SAGA Light Source.

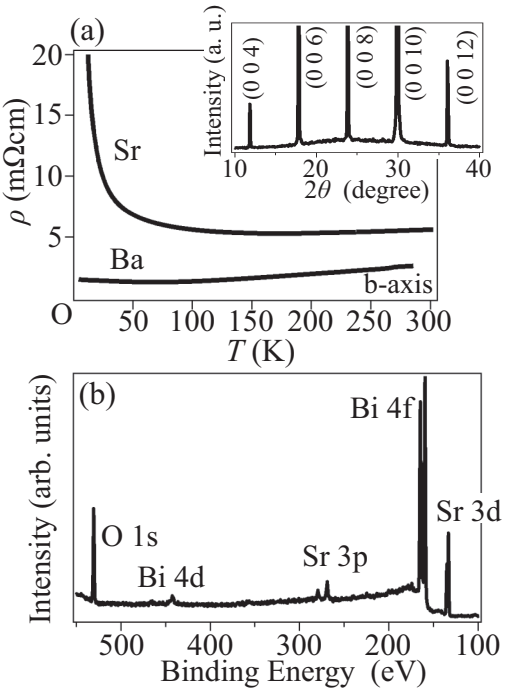

FIG. 1. (a) Temperature dependence of the in-plane resistivity of BSCO and BBCO. Inset: X-ray $(0,0,l)$ diffraction patterns measured using Cu $K\alpha$ radiation. (b) Core-level photoemission spectra ($h\nu = 680$ eV) of the BSCO.

Samples cleaved *in situ* were measured at base pressures of higher than 10^{-10} Torr. The surface cleanliness was checked on the basis of core-level photoemission spectra measured using synchrotron radiation. Figure 1(b) shows that contaminants such as carbons were negligibly small on the sample surface. ARPES measurements were conducted using synchrotron radiation with a photon energy of 100 eV. The typical energy and angular resolutions were, respectively, 35 meV and 0.8°. The Fermi level E_F of the sample was referenced to that of polycrystalline gold.

III. RESULTS AND DISCUSSION

Figure 2(a) presents a comparison of the angle-integrated photoemission spectra of BBCO and BSCO at several temperatures. The spectra are integrated over the area of a circle with a radius of $k = 0.65$ Å^{-1} around the Γ point. The basic similarity in the spectral forms is readily apparent. A quasiparticle peak and finite spectral intensity at E_F are visible in BBCO, which shows good agreement with descriptions in previous reports [19–21]. In contrast, in BSCO, a clear suppression of spectral weight exists near E_F. This is a phenomenon called the pseudogap [4]. As shown in the enlarged view in Fig. 2(b), with decreasing temperature, the intensity in the gap region decreases gradually. Suppression of the density of state near E_F is consistent with transport measurements in $[Bi_2Sr_2O_4]_pCoO_2$: The resistivity increases as the temperature decreases.

Figure 3(a) presents a plot of ARPES intensity around E_F in BBCO as a function of a two-dimensional wave vector, taken at 20 K. The first Brillouin zone (BZ) of the triangular

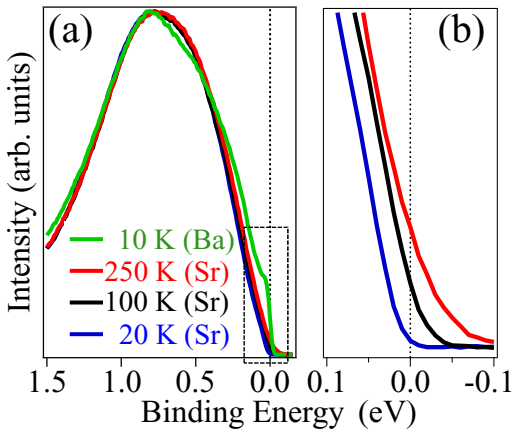

FIG. 2. (a) Photoemission spectra ($h\nu = 100$ eV) of BBCO and BSCO at various temperatures. Spectra are integrated over the area of a circle with a radius of $k = 0.65$ Å^{-1} around the Γ point. (b) Enlarged view of the rectangular area in (a) for BSCO.

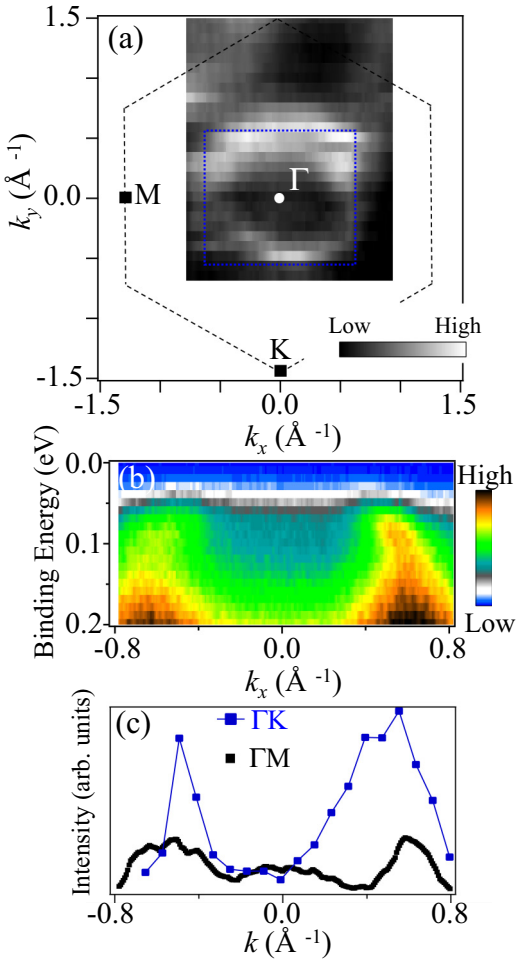

FIG. 3. (a) Plots of ARPES intensity of BBCO as a function of k_x and k_y. Data were taken at 20 K and integrated over the energy range of ±15 meV with respect to E_F. The dashed line corresponds to the BZ of the CoO_2. (b) Plots of ARPES intensity as a function of binding energy and wave vector. Measurements are performed along the high-symmetry line ΓM. (c) Intensity profiles along the ΓM and ΓK directions.

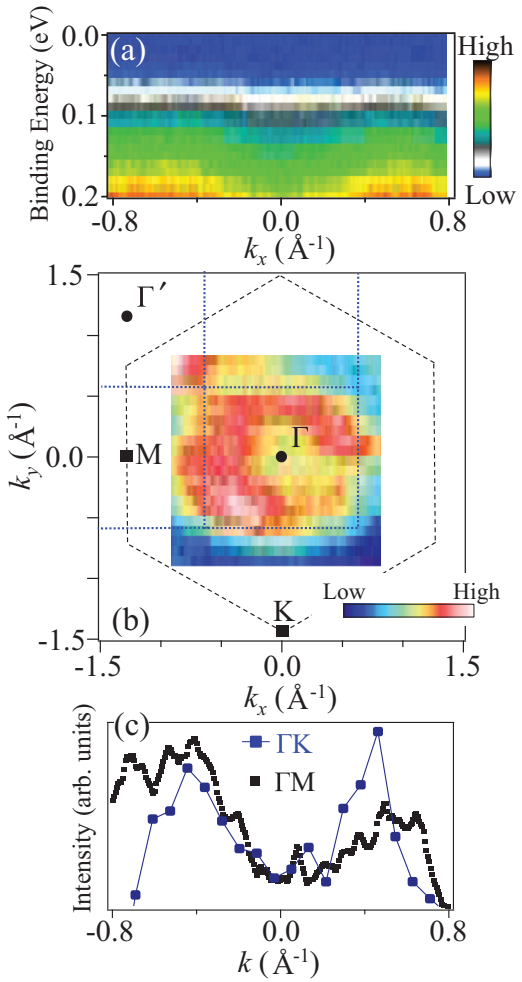

FIG. 4. (a) Plots of ARPES intensity measured at 20 K along the ΓM direction in BSCO. (b) Intensity map integrated over the energy range of ± 15 meV with respect to E_F. The dashed and dotted lines respectively present the BZ of the CoO_2 and the RS sublattices. (c) Intensity profiles along the ΓM and ΓK directions.

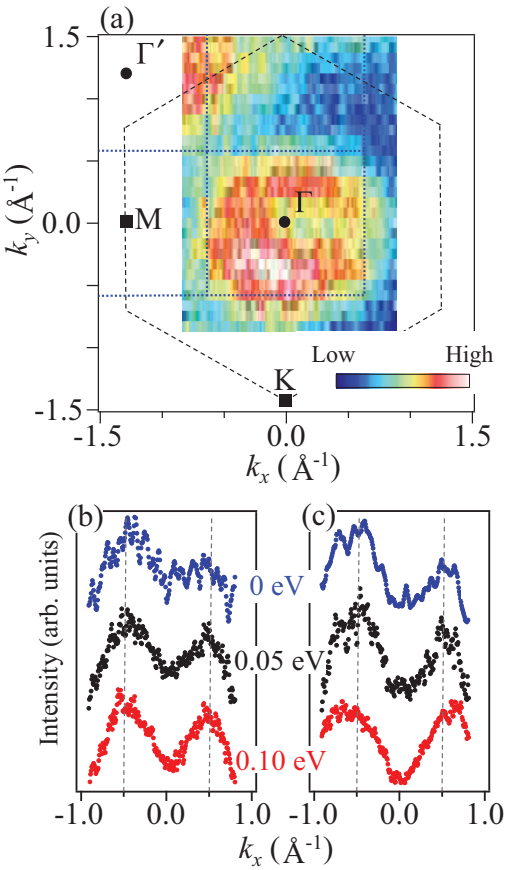

FIG. 5. (a) The ARPES intensity map around E_F of BSCO measured at 300 K. Intensity profiles along the ΓM direction (b) at 300 K and (c) at 20 K at three different binding energies.

CoO_2 lattice is also shown (dashed line) as a guide. The observed FS is as large as or slightly smaller than the first BZ of the RS lattice drawn by a blue dotted line. This result shows good agreement with previous reports [16,19]: A large FS exists centered at the Γ point. Figure 3(b) shows ARPES intensity plots along the high-symmetry line ΓM. The dispersion relation reveals that the FS is holelike and that it is mainly constructed from the a_{1g} orbital, as predicted by the band structure calculations [22,23]. The local maxima of the intensity profiles along the ΓM and ΓK directions, respectively, give Fermi wave numbers k_F of 0.56 and 0.47 Å^{-1} [Fig. 3(c)]. Assuming a simple hexagonal FS of the a_{1g} band, the hole concentration is roughly estimated as 2×10^{21} cm^{-3}. This value agrees with that deduced from the Hall effect measurement [15], suggesting that cobalt ions exist as a mixture of Co^{3+} and Co^{4+}, and Luttinger's theorem is valid for BBCO.

Figure 4(a) shows the ARPES intensity plots along the ΓM direction at 20 K in BSCO. Although we find a holelike dispersion centered at the Γ point, it is broader than that of BBCO [see Fig. 3(b)]. The intensity near E_F is reduced strongly, indicating the presence of a pseudogap. Even in the pseudogap regime, the spatial intensity distribution remains. Figure 4(b) shows the k-space mapping of the ARPES intensity around E_F. The high-intensity region forms a hexagonal shape, which resembles the FS of BBCO shown in Fig. 3(a). It is noteworthy that another high-intensity region is apparent at the upper left-hand side of the image. This position corresponds to that in which the central hexagon is translated by RS periodicity indicated by blue dotted lines. Consequently, the existence of the replica demonstrates that the observed intensity distribution is attributed to the FS and indicates coupling between the CoO_2 and RS structures as described for BBCO [16,17]. The Fermi wave numbers k_F are 0.57 and 0.46 Å^{-1}, respectively, for the ΓM and ΓK directions from the momentum distribution curves, as shown in Fig. 4(c). According to Luttinger's theorem, the carrier concentration in BSCO is expected to be comparable to that in BBCO, which is contrary to both the higher resistivity and the localization behavior observed for BSCO.

It is particularly interesting that the FS size is temperature dependent. The k-space plot of ARPES intensity around E_F obtained at 300 K is shown in Fig. 5(a). In spite of the thermal smearing of the Fermi function, the hexagonal FS and its replica are still readily apparent. In comparison to Figs. 4(b)

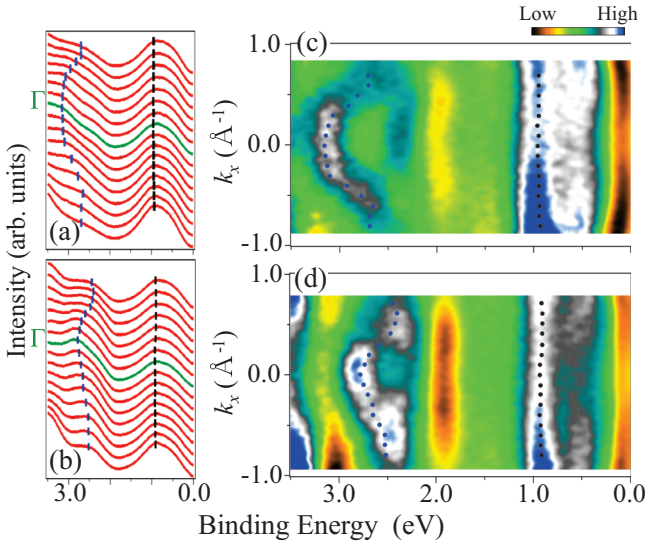

FIG. 6. Energy distribution curves along the Γ*M* direction of BSCO measured (a) at 300 K and (b) at 20 K. The blue and black dashed bars are guides to the eyes to trace the peak positions. Second derivatives of ARPES spectra (c) at 300 K and (d) at 20 K.

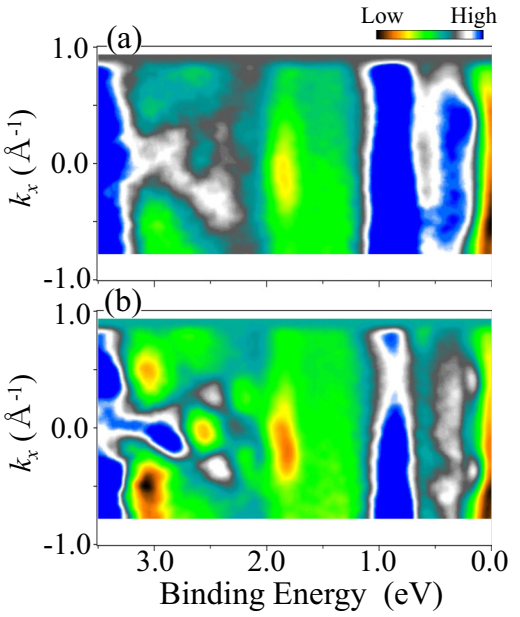

FIG. 7. Second derivatives of ARPES spectra along the Γ*M* direction of BBCO (a) at 300 K and (b) at 20 K.

and 5(a), it is apparent that the contour of the FS shrinks with increasing temperature. Figures 5(b) and 5(c) respectively portray the intensity profiles at three different energies of 0 (E_F), 0.05, and 0.10 eV, obtained at 300 and 20 K. The peak position varies with temperature, which is more clearly visible at the higher-energy (higher-intensity) level. According to the Drude model, the smaller FS in the more conductive region signifies that an anomalous change in the scattering rates of charge carriers occurs in BSCO. However, possible correlation effects among electrons are unlikely because the FS shape is not drastically altered by temperature.

To further elucidate the origin of the unusual behavior, the band structure in the higher-energy range up to 3.5 eV was specifically addressed. Figures 6(a) and 6(b) respectively portray the energy distribution curves along the Γ*M* direction obtained at 300 and 20 K. Blue and black dashed bars are guides to the eyes to trace the peak positions. A comparison of the two figures reveals no great difference in spectral structure for binding energies of 0–1.0 eV. At energies higher than 2.0 eV, however, it is noteworthy that the valence band structure is modified considerably, as shown clearly in the second derivatives of the ARPES spectra presented in Figs. 6(c) (300 K) and 6(d) (20 K). In the electronic structure at 20 K, the bottom of the band denoted by the blue markers is shifted by about 0.25 eV compared with that at 300 K. Such a tendency is not observed for BBCO, as shown in Figs. 7(a) (300 K) and 7(b) (20 K). Consequently, in BSCO, the band structure is not rigid but it is quite sensitive to temperature variations.

In incommensurate $Bi_2Ba_{1.3}K_{0.6}Co_{2.1}O_{7.94}$, previous reports show that the corresponding valence structure is sensitive to the photon energy [16], which indicates the presence of an interaction between the CoO_2 and RS sublattices. Consequently, our observations suggest that the change in the intersublattice coupling is induced by temperature. Figure 8 portrays the oxygen 1*s* core-level spectra of BSCO at different temperatures, together with the cobalt $2p_{1/2}$ and $2p_{3/2}$ spectra (inset). The oxygen core-level binding energy is shifted by about 0.2 eV at the low temperature, which cannot be determined in the case of the cobalt peaks within the resolution. Therefore, the remarkable modification of the band structure is closely related to the change in the orbital energies of the oxygen atoms, i.e., the chemical environment around the oxygen atoms is modified by changing temperature. No structural transition has been found in BSCO. Therefore, the most probable cause is the local structural deformations because of the misfit strain. Actually, we directly observed short-range corrugations in the RS structure, probably induced by the mismatch with the CoO_2 one, via STM measurements [18]. The presence of inequivalent oxygen sites in the RS lattice influences the electronic states of the adjacent CoO_2 layer: the splitting of the 3*d* orbitals of the cobalt ions. Particularly, the a_{1g} level is expected to be affected because the a_{1g} orbital spreads along the *c* direction. Consequently, its energy level is broadened, leading to the loss of coherent spectral weight (formation of the pseudogap).

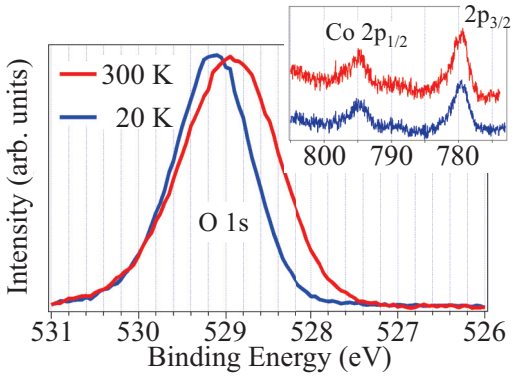

FIG. 8. Oxygen 1*s* core-level photoemission spectra of BSCO ($h\nu = 680$ eV). Inset: Cobalt $2p_{1/2}$ and $2p_{3/2}$ spectra ($h\nu = 1080$ eV).

Our experiments demonstrate that no definite energy gap exists in the pseudogap state of BSCO. Neither the electron correlation nor the Hume-Rothery mechanism expected for aperiodic systems is the cause of the unusual behavior because the shape of the FS does not change much. We propose that the temperature dependence of the electronic properties is attributable to a mismatch of the thermal expansion coefficient between the CoO_2 and RS sublattices. A similar proposal has been made for a misfit-layered chalcogenide, $(LaS)_{1.196}VS_2$, in which vanadium clusters are expected to be deformed with temperature [24]. The temperature-dependent local structure for a misfit-layered calcium cobaltite $[Ca_2CoO_3][CoO_2]_{1.61}$ ($Ca_3Co_4O_9$) has also been discussed [25]. The materials, which consist of flexible stacks of layers, are expected to be a subject of study in condensed matter physics. Further research must be undertaken to elucidate the fundamental properties and the emergence of new functional properties.

IV. CONCLUSIONS

We conducted ARPES measurements for two types of cobaltites, $[Bi_2Ba_2O_4]_{0.50}CoO_2$ (BBCO) and $[Bi_2Sr_2O_4]_pCoO_2$ (BSCO). The photoemission spectra of BSCO showed a pseudogap structure, whereas a finite spectral intensity existed at E_F in BBCO. Even in the pseudogap region of BSCO, the FS could be mapped out from the nonuniformity in the photoelectron intensity distribution. The FS size was altered with temperature, but the FS shape does not change greatly. In addition, following a temperature change, we observed a modification of the high-energy part of the spectra. These results suggest that the local structural deformations cause the pseudogap phenomenon. The anomalous temperature dependence can be attributed to the mismatch of thermal expansion coefficients between the two sublattices of the incommensurate crystal structure.

[1] I. Terasaki, Y. Sasago, and K. Uchinokura, Phys. Rev. B **56**, R12685 (1997).

[2] A. C. Masset, C. Michel, A. Maignan, M. Hervieu, O. Toulemonde, F. Studer, B. Raveau, and J. Hejtmanek, Phys. Rev. B **62**, 166 (2000).

[3] R. Funahashi, I. Matsubara, and S. Sodeoka, Appl. Phys. Lett. **76**, 2385 (2000).

[4] T. Takeuchi, T. Kondo, T. Takami, H. Takahashi, H. Ikuta, U. Mizutani, K. Soda, R. Funahashi, M. Shikano, M. Mikami, S. Tsuda, T. Yokoya, S. Shin, and T. Muro, Phys. Rev. B **69**, 125410 (2004).

[5] M. L. Foo, Y. Wang, S. Watauchi, H. W. Zandbergen, Tao He, R. J. Cava, and N. P. Ong, Phys. Rev. Lett. **92**, 247001 (2004).

[6] I. R. Mukhamedshin, H. Alloul, G. Collin, and N. Blanchard, Phys. Rev. Lett. **93**, 167601 (2004).

[7] W. Koshibae and S. Maekawa, Phys. Rev. Lett. **91**, 257003 (2003).

[8] W. B. Wu, D. J. Huang, J. Okamoto, A. Tanaka, H.-J. Lin, F. C. Chou, A. Fujimori, and C. T. Chen, Phys. Rev. Lett. **94**, 146402 (2005).

[9] J. Chaloupka and G. Khaliullin, Phys. Rev. Lett. **99**, 256406 (2007).

[10] I. Tsukada, T. Yamamoto, M. Takagi, T. Tsubone, S. Konno, and K. Uchinokura, J. Phys. Soc. Jpn. **70**, 834 (2001).

[11] J. Bobroff, S. Hébert, G. Lang, P. Mendels, D. Pelloquin, and A. Maignan, Phys. Rev. B **76**, 100407(R) (2007).

[12] S. P. Bayrakci, C. Bernhard, D. P. Chen, B. Keimer, R. K. Kremer, P. Lemmens, C. T. Lin, C. Niedermayer, and J. Strempfer, Phys. Rev. B **69**, 100410(R) (2004).

[13] J.-M. Tarascon, R. Ramesh, P. Barboux, M. S. Hedge, G. W. Hull, L. H. Greene, M. Giroud, Y. LePage, W. R. McKinnon, J. V. Waszcak, and L. F. Schneemeyer, Solid State Commun. **71**, 663 (1989).

[14] H. Alloul, I. R. Mukhamedshin, T. A. Platova, and A. V. Dooglav, Europhys. Lett. **85**, 47006 (2009).

[15] S. Hébert, W. Kobayashi, H. Muguerra, Y. Bréard, N. Raghavendra, F. Gascoin, E. Guilmeau, and A. Maignan, Phys. Status Solidi A **210**, 69 (2013).

[16] H. W. Ou, J. F. Zhao, Y. Zhang, B. P. Xie, D. W. Shen, Y. Zhu, Z. Q. Yang, J. G. Che, X. G. Luo, X. H. Chen, M. Arita, K. Shimada, H. Namatame, M. Taniguchi, C. M. Cheng, K. D. Tsuei, and D. L. Feng, Phys. Rev. Lett. **102**, 026806 (2009).

[17] A. Nicolaou, V. Brouet, M. Zacchigna, I. Vobornik, A. Tejeda, A. Taleb-Ibrahimi, P. Le Fèvre, F. Bertran, C. Chambon, S. Kubsky, S. Hébert, H. Muguerra, and D. Grebille, Europhys. Lett. **89**, 37010 (2010).

[18] M. Maki, S.-I. Takakura, T. Nishizaki, and F. Ichikawa, Phys. Rev. B **92**, 165117 (2015).

[19] V. Brouet, A. Nicolaou, M. Zacchigna, A. Tejeda, L. Patthey, S. Hébert, W. Kobayashi, H. Muguerra, and D. Grebille, Phys. Rev. B **76**, 100403(R) (2007).

[20] A. Nicolaou, V. Brouet, M. Zacchigna, I. Vobornik, A. Tejeda, A. Taleb-Ibrahimi, P. Le Fèvre, F. Bertran, S. Hébert, H. Muguerra, and D. Grebille, Phys. Rev. Lett. **104**, 056403 (2010).

[21] V. Brouet, A. Nicolaou, M. Zacchigna, A. Taleb-Ibrahimi, P. Le Fèvre, and F. Bertran, J. Electron Spectrosc. **185**, 146 (2012).

[22] D. J. Singh, Phys. Rev. B **61**, 13397 (2000).

[23] P. Zhang, W. Luo, M. L. Cohen, and S. G. Louie, Phys. Rev. Lett. **93**, 236402 (2004).

[24] V. Ta Phuoc, V. Brouet, B. Corraze, E. Janod, M. Zaghrioui, and L. Cario, J. Phys. Chem. C **118**, 19273 (2014).

[25] T. A. Tyson, Z. Chen, Q. Jie, Q. Li, and J. J. Tu, Phys. Rev. B **79**, 024109 (2009).